Ionization processes in small quasimolecules: He_2^{2+} (He^{2+} + He)

G. N. Ogurtsov,[1] S. Yu. Ovchinnikov,[1,2,3] J. H. Macek,[2,3] and V. M. Mikoushkin[1]
[1]*Ioffe Physico-Technical Institute, 194021 St. Petersburg, Russia*
[2]*Department of Physics and Astronomy, University of Tennessee, Knoxville, Tennessee 37996-1501, USA*
[3]*Oak Ridge National Laboratory, P.O. Box 2009, Oak Ridge, Tennessee 37831, USA*
(Received 3 January 2011; published 7 September 2011)

The energy spectra of electrons ejected in He^{2+}−He collisions were measured in the ion energy range 6–30 keV. Theoretical analysis of the ionization mechanisms has been performed on the basis of the advanced adiabatic approximation for one-electron processes and perturbation theory for two-electron processes. The ionization channel $2p\sigma^2 \rightarrow 1s\sigma nd\sigma \rightarrow 1s\sigma\varepsilon d\sigma$ has been revealed, which makes a considerable contribution to the ionization cross section in the keV ion energy range.

DOI: 10.1103/PhysRevA.84.032706 PACS number(s): 34.50.Fa

I. INTRODUCTION

In recent years, considerable progress has been achieved in quantitative theoretical descriptions of dynamical processes (such as ionization) in which one "active" electron is involved [1]. Very accurate calculations of such processes have become feasible in a wide range of collision energies. Now the challenge is shifted toward the quantitative study of the dynamical processes, which cannot be described by one-electron approximations, and electron correlations should be taken into account.

The quasimolecule He_2^{2+} (He^{2+} + He) is one of the simplest quasimolecular systems with two electrons accessible for experimental and theoretical study. Experimentally, the total cross sections for ionization were measured earlier by the condenser method [2] and by the "ejected electron–recoil ion" coincidence technique [3,4]. Elementary processes occurring in He^{2+}−He collisions were investigated using the "scattered ion–recoil ion" coincidence technique [5]. A compilation of the data is given in the handbook [6] where recommended values of cross sections are suggested. Electron energy distributions in arbitrary units were measured in Ref. [7] at one particular ion energy. The production of some doubly excited autoionization states in high-energy He^{2+}-He collisions was studied in Ref. [8] using electron spectroscopy.

In the past decade much progress has been made in measuring electron and residual ion momentum distributions via cold target recoil ion momentum spectroscopy (COLTRIMS) [9–14]. As a rule, such experiments were performed at high incident ion energy. Theoretical study of autoionization in the quasimolecule He_2^{2+} was performed in Refs. [15–21]; potential energy curves, energy widths, and cross sections for excitation of some of the lowest autoionization states were calculated. However, a complete understanding of the dynamics of ionization processes in the quasimolecule He_2^{2+} was not achieved until now. In particular, the available experimental data do not allow estimating contributions of one-electron (direct ionization) and two-electron (autoionization) processes to the total ionization cross section. Indeed, in the quasimolecular approximation, both processes populate the degenerate final states He^2 + (projectile) + He^+(target) [process 2021] and He^+(projectile) + He^{2+}(target) [process 2012]. Thus, the data on the cross sections for processes 2021 and 2012 obtained in the coincidence experiments do not enable distinguishing between direct ionization and autoionization in He^{2+}-He collisions. Moreover, the total cross sections for ionization of a target atom obtained in Ref. [6] by extrapolation of experimental data to lower ion energies are of the order of 10^{-19} cm^2, while the calculations of autoionization [17] and measurements of the total ionization cross sections [4] give the values of the order of 10^{-17} cm^2.

In the present paper we have attempted to clarify the situation by studying energy spectra of electrons ejected in He^{2+}−He collisions, which can provide detailed information on the ionization mechanism. In addition, the programs of calculations of two-electron transitions in quasimolecules developed at the Oak Ridge National Laboratory make it possible to consider a great number of ionization channels.

II. EXPERIMENTAL TECHNIQUE

The doubly differential cross sections were measured using our electron spectrometer described elsewhere [22,23]. A schematic view of the experimental setup is shown in Fig. 1.

An ion beam from an ion source of duoplasmatron type (IS), after passing through the magnet mass separator (M) and quadrupole lenses (QL), entered a gas cell placed inside the inner electrode of the cylindrical electrostatic mirror analyzer (A) with the entrance angle $\theta = 54.5^{\circ}$ and the energy resolution $\Delta E/E = 0.63\%$. The inner electrode (grounded) was made of a uniform brass cylinder and had entrance and exit slits with an effective length of 0.3 mm. The outer electrode (under analyzing potential) was made of tungsten mesh with a transparency of 98.5%. The whole analyzer volume was surrounded by a uniform brass screen. The primary beam current was measured by a Faraday cup with guard rings, placed inside the inner electrode after the gas cell. An array of guard rings (Solter rings) was installed in the collision chamber to avoid penetration of electrons from surfaces into the analyzer volume. The energy-analyzed electrons were directed to a detector (D) consisting of a channeltron and a dispersion element used for discrimination against spurious electrons. In measuring Auger electron spectra, this dispersion element was represented by a small low-resolution cylindrical mirror (shown in Fig. 1), while in studying the low-energy part of the spectrum a small conical deflector was used. The electron spectra were normalized to the primary ion beam

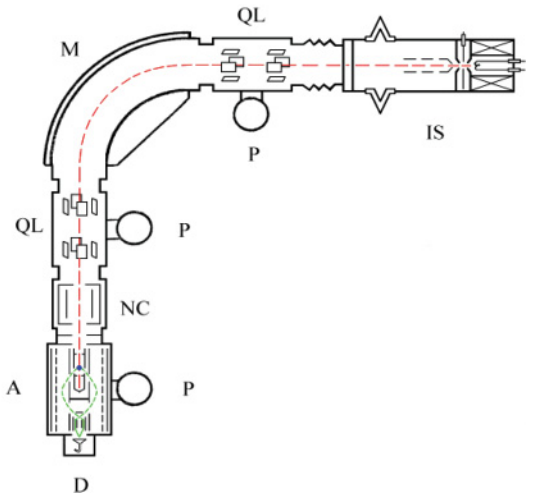

FIG. 1. (Color online) Experimental setup: IS, ion source; QL, quadrupole lenses; M, magnet mass separator; NC, neutralization chamber; A, electron energy analyzer; P, diffusion pumps.

by converting the electrometer data into a series of pulses (with the aid of a current-to-frequency converter), which were then counted. Stray magnetic fields were reduced to less than 10 mG by using nonmagnetic materials, μ-metal shielding, and compensation by three pairs of Helmholtz coils. The isotope $^3He^{2+}$ was used to separate it from H_2^+. The helium pressure in the collision chamber was 4×10^{-4} Torr, and the pressure of the residual gas did not exceed 2×10^{-6} Torr. The single-collision regime was maintained.

Absolute values of the doubly differential cross sections are determined by the relation

$$\frac{d^2\sigma}{dE_e d\Omega} = \frac{K}{n}\left(\frac{N_e}{N_i}\right), \quad K = \frac{1}{\Delta E \eta \int \Omega dl}, \tag{1}$$

where n is the target gas density, ΔE is the absolute energy resolution (full width at half maximum), η is the detection efficiency, $\int \Omega dl$ is a geometric factor characterizing the electron ejection solid angle and collection length, and N_e and N_i are the fluxes of electrons and incident ion beams, respectively.

The parameters and constants entered in expression (1) were determined both from control experiments and from calibration to the well-established data available in the literature (in particular, the data [24] on electron impact). The following control experiments were performed.

A. Geometrical factor $\int \Omega dl$

In this series of control experiments, a small electron gun was installed inside the inner electrode, directed at an angle of 54.5° with respect to the analyzer axis, that could move along the axis. The electron current as a function of the gun position was measured by a Faraday cup located behind a cut in the analyzer screen, opposite to the entrance slit, to give the geometrical factor, which can also be determined from geometrical calculation. The result obtained was $\int \Omega dl = (3.7 \pm 0.3) \times 10^{-3}$ cm sr.

B. Registration efficiency η

In these control experiments, the small electron gun was used as well. The electron current was measured both by the Faraday cup located behind the cut and by the Faraday cup placed instead of the channeltron in the detector. By this manner, the analyzer transparency α was determined. The channeltron registration efficiency β was measured in a separate experiment in which the channeltron acted both as a Faraday cup and in the counting regime. The result obtained was $\eta = \alpha\beta = 0.74 \pm 0.05$, at $E_e > 4$ eV. The operation regime of the detector was chosen in such a way to maintain a plateau in dependence of the electron signal on the potentials applied to the channeltron and guard rings.

C. Gas pressure

The gas pressure was measured by an ionization gauge calibrated by the McLeod gauge in a standard manner. The uncertainty of these measurements was ±15%.

D. Analyzer calibration

The true energy of ejected electrons is determined by the relation $eV_0 = k(eV_A + eV_C)$, where eV_A and eV_C are the analyzer potential and the contact potential, respectively. The values of k and V_C were determined by comparing measured positions of two spectral lines whose positions are well known from spectroscopic data. (We usually used Auger spectrum for e-Xe collisions). The result obtained was $k = 0.993 \pm 0.003$, $V_C = 0.16$ V.

E. Energy resolution

The energy resolution of the analyzer was determined using the following three methods:

(i) comparison to the width of a line from a source of electrons with fixed energy,

(ii) comparison to the width of a peak for electron elastic scattering, and

(iii) comparison to the width of a line of the Auger spectra with well-known natural width.

The result obtained was $\Delta E/E = (0.63 \pm 0.05)\%$. The combination of the above errors gives a total uncertainty of measurements of the absolute cross sections of about 20%. The calibration procedure gives the same value.

The measurements were performed in the ion energy range 6–30 keV and in the ejected electron energy range 5–70 eV.

III. THEORY

A. Energies and widths

For the analysis of the studied processes, it was necessary to calculate two-electron molecular potential curves and probabilities for two-electron transitions, particularly autoionization. The product of one-electron molecular wave functions was used as the basis for two-electron wave functions. The calculations of bound-state one-electron molecular wave functions, ψ_{Ei}, and molecular eigenvalues, E_i, were performed using a standard procedure of solving the Schrödinger equation in prolate spheroidal coordinates [25]. The quasiradial parts of

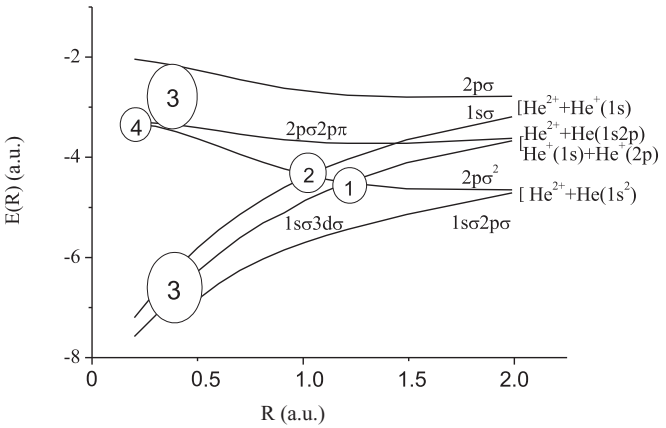

FIG. 2. Potential energy curves of the system He_2^{2+}. (The term $4/R$ is subtracted.) characteristic regions of internuclear distance are indicated.

the bound-state functions were expressed by Jaffe expansions with normalization of the total wave function to unity at each internuclear distance R. The quasiradial parts of the continuum wave functions, ψ_ε, where ε is the energy of the continuum state, were obtained from numerical integration of the Schrödinger equation and normalized to an energy δ function. The quasiangular wave functions in both cases were expressed by the expansions over Legendre polynomials. The matrix elements for two-electron transitions,

$$V_{12}(R) = \langle \psi_{E1}(1)\psi_{E2}(2)| \frac{1}{|\mathbf{r}_1 - \mathbf{r}_2|} |\psi_{E3}(1)\psi_{E4}(2)\rangle, \quad (2)$$

were evaluated in the Fourier space, where (1,2) indicates a manifold of coordinates of electron 1 or electron 2. The results obtained on the potential energy curves and the widths of the lowest autoionization states are shown in Figs. 2 and 3. The potential curves for the states $2p\pi^2$ and $2s\sigma^2$ are not shown in Fig. 2, to avoid overcomplicating the figure. Our results on the potential curves agree to within a few percent of the previous calculations [16]. The data obtained on the widths, $\Gamma(R) = 2\pi|V_{12}(R)^2|\ \delta(E_1 + E_2 - E_3 - \varepsilon)$, agree with the calculations [16,18] within 15%.

The wave functions $\psi_{Ei}(R)$ for $i = 1, 2, 3$ in the matrix element $V_{12}(R)$ are the bound-state wave functions and $\psi_{E4}(R) = \psi_\varepsilon(R)$ is the continuum wave function.

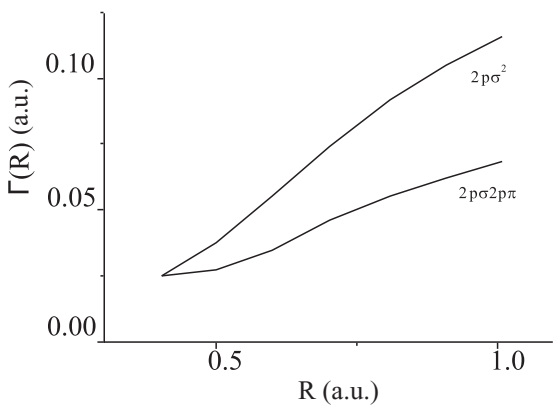

FIG. 3. Widths of autoionization states of the quasimolecule He_2^{2+}.

The initial state, $He^{2+} + He\ (1s^2)$, correlates to the quasimolecular terms $^1\Sigma_g{}^+\ (2p\sigma^2)$ and $^1\Sigma_u{}^+\ (1s\sigma 2p\sigma)$ (see, e.g., discussion in Ref. [26]). In approaching colliding particles, these terms pass through the following characteristic regions (Fig. 2):

(i) $R = 1.2$–1.4 a.u. In this region the initial diabatic potential curve $^1\Sigma_g^+\ (2p\sigma^2)$ crosses the potential curve $^1\Sigma_g^+\ (1s\sigma 3d\sigma)$.

(ii) $R < 1.06$ a.u. In this region, the diabatic potential curve $^1\Sigma_g^+\ (2p\sigma^2)$ crosses the boundary of continuum $1s\sigma$ and becomes an autoionizing one.

(iii) $R = 0.4$–0.5 a.u. In this region, superpromotion of the initial diabatic potential curves $2p\sigma^2$ and $1s\sigma 2p\sigma$ occurs, resulting in direct ionization.

(iv) $R = 0.2$–0.3 a.u. In this region, formation of the doubly excited states $2s\sigma^2$, $2p\sigma 2p\pi$, $2p\pi^2$, etc., is most effective.

IV. DIRECT IONIZATION

Cross sections for direct ionization are calculated using the advanced adiabatic approximation [27]. In this approximation, the differential cross section for electron ejection is written as

$$\frac{d\sigma}{dE} = \frac{4\pi\,|R(E)|^2\,\mathrm{Im}R(E)}{\alpha(E)} \exp\left[-\frac{\alpha(E)}{v}\right], \quad (3)$$

where $\alpha(E) = 2\int^E \mathrm{Im}R(E')dE'$ and $R(E)$ is the function reciprocal to $E(R)$. The complex function $R(E)$ was determined by scaling of the analogous function for the system $H_2{}^+$ (Eq. (6) of Ref. [27]), with the effective charge chosen to provide the correct value of the binding energy of the ionized electron in the united atom limit.

A. Quasimolecular autoionization

The cross section for electron ejection via an autoionization process can be written as

$$\frac{d\sigma}{dE} = 2\pi \int_0^\infty N(b,R(E))W(E,b)bdb, \quad (4)$$

where b is the impact parameter, $N(b,R)$ is the population of the autoionization state, and $W(E,b)$ is the autoionization transition probability determined using the perturbation

$$W(E,b) = \left| \int^\infty \sqrt{\frac{\Gamma(t')}{2\pi}} \exp\left\{ iEt\prime - i\int^{t'} E_0(t'')dt'' \right\} dt' \right|^2, \quad (5)$$

where $E_0(t)$ is the energy of the autoionization state counted with respect to the final-state energy, and $\Gamma(t)$ is the energy width. If $\Gamma\,(t) \ll 1$ then Eq. (5) can be reduced to (see, e.g., Ref. [28]):

$$W(E,b) \cong \frac{\Gamma(t_0)}{E_t'(t_0)} = \frac{\Gamma(R_0)}{v_R E_R'(R_0)}, \quad (6)$$

where $E_t' = dE/dt$, $E_R' = dE/dR$, t_0 and R_0 are the time and internuclear distance corresponding to the stationary phase point determined by the condition $E = E_0(t_0)$, v_R is the radial

velocity, and the differential cross section Eq. (4) can be written as

$$\frac{d\sigma}{dE} \cong \frac{I(R_0)\Gamma(R_0)}{vE'_R(R_0)}, \tag{7}$$

where

$$I(R_0) = \int_0^\infty \frac{N(b,R_0)bdb}{v_R(R_0)/v}. \tag{8}$$

In calculating the cross sections, we used our own values of $\Gamma(R)$ as well as the data on $N(b,R)$ taken from Ref. [17].

The function $I(R)$ for the state $2p\sigma^2$ was found to obey the relation $I(R) = 0.027\exp(4R)$ (a.u.). The analogous function for the state $2p\sigma 2p\pi$ was found to equal 0.14 a.u. at all electron energies in the range 5–30 eV.

When determining the doubly differential cross sections, expressions (3) and (4) should be multiplied by a certain function $f(E,\Omega)$ characterizing the angular distribution of ejected electrons. Our calculations have shown that in the case under study the angular distribution in the center-of-mass frame can be considered isotropic in a wide range of electron energies. Therefore, the cross sections in the laboratory frame can be obtained by dividing the cross sections (3) and (4) by 4π and taking the values determined by kinematic relations between these two coordinate systems (see, e.g., Ref. [29]):

$$\begin{aligned} \sigma''_{\rm lab} &= (1 - 2\delta\cos\theta_{\rm lab} + \delta^2)^{-1/2}\sigma''_{\rm c.m.}, \\ E_{\rm c.m.} &= (1 - 2\delta\cos\theta_{\rm lab} + \delta^2)E_{\rm lab}, \end{aligned} \tag{9}$$

where $\sigma'' = d^2\sigma/dEd\Omega$, $\delta = v_{\rm c.m.}/v_{\rm lab}$.

V. RESULTS AND DISCUSSION

A. Differential cross sections

Figure 4 shows energy spectra of electrons ejected in $^3He^{2+}-^4He$ collisions measured at the ejection angle $\theta = 54.5^\circ$ and at the ion energies 6 and 12 keV. One can discern the following features of the spectra: the continuous part of the spectrum dominating at low electron energies, a very broad continuous band dominating at higher energies, and a discrete structure connected with autoionization transitions in separated target and projectile (the latter is shifted to higher energies due to the Doppler effect).

Of particular interest is the low-energy part of the spectrum ($E_e < 10$ eV). In the ion energy range under study the doubly differential cross sections exhibit behavior typical for the direct-ionization cross sections; i.e., they increase with increasing ion energy and exponentially decrease with increasing electron energy. However, our calculation of the doubly differential cross sections (Fig. 5, curve D2 + D3) as well as the available data on the total cross sections for direct ionization (e.g., Ref. [6]) show that the contributions of the known channels for direct ionization are too small to explain the low-energy part of the spectrum. This may imply that one more channel for direct ionization exists at medium internuclear distances that was not taken into account in previous studies. Such a direct-ionization channel associated with two-electron transitions $2p\sigma^2$-$1s\sigma 3d\sigma$ have been found.

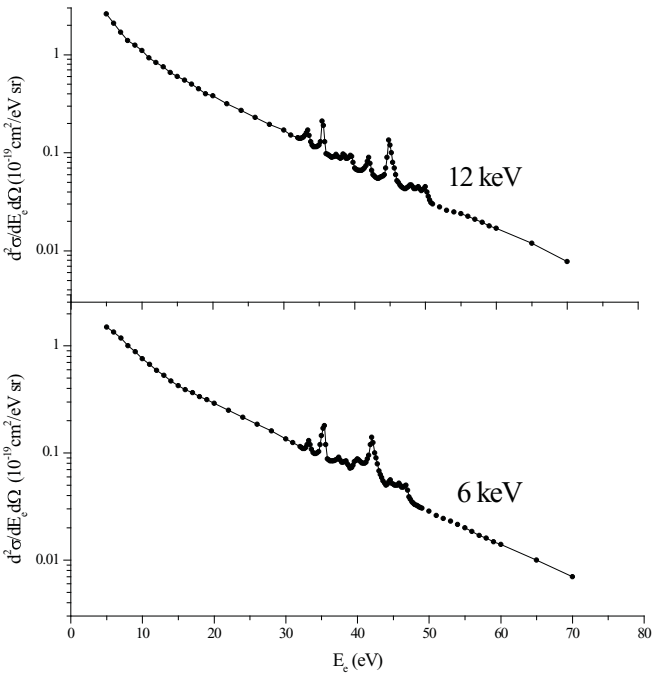

FIG. 4. Energy spectra of electrons ejected in $^3He^{2+}-^4He$ collisions.

B. Direct ionization

The following channels for direct ionization have been considered:

$$\text{(D1)}\ 2p\sigma^2 \rightarrow 1s\sigma 3d\sigma \rightarrow 1s\sigma\varepsilon d\sigma, \tag{10}$$

$$\text{(D2)}\ 2p\sigma^2 \rightarrow 2p\sigma\varepsilon p\sigma, \tag{11}$$

$$\text{(D3)}\ 1s\sigma 2p\sigma \rightarrow 1s\sigma\varepsilon p\sigma. \tag{12}$$

The channels (11) and (12) are associated with S ionization (superpromotion [30]) of the initial states to continuum at small

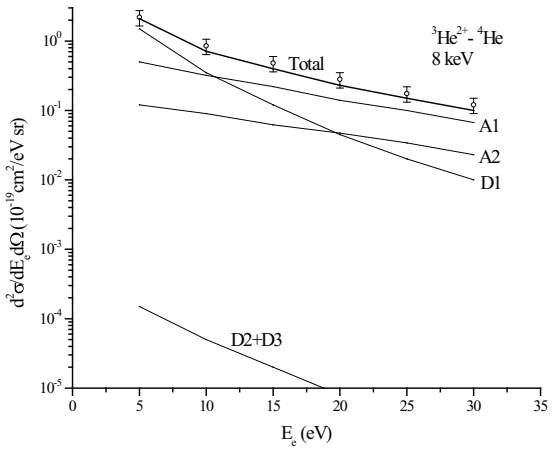

FIG. 5. Doubly differential cross sections for ejection of electrons in He^{2+}-He collisions at 8 keV. Labels near curves indicate the contributions of different channels and the bold line indicates the sum of all contributions. Circles represent experimental data.

internuclear distances. Their contribution was calculated using the advanced adiabatic approximation, Eq. (3).

The newly discovered channel (10) proceeds in two steps: two-electron coupling of terms followed by one-electron superpromotion. The probability for the first step can be estimated using the Landau-Zener formula,

$$P(v) = 1 - \exp\left(-\frac{4\pi V_{1,2}^2}{v E_R'}\right) \equiv 1 - \exp\left(-\frac{a}{v}\right), \quad (13)$$

where E_R' equals the difference of slopes of the crossing potential curves. The matrix element for two-electron transition $V_{1,2} = V_{12}(R_1)$ determined by Eq. (2) was evaluated with the wave functions $\psi_{Ei}(R_1)$ for $i = 1,2,3,4$ corresponding to bound states at the crossing point R_1, where $E_1(R_1) + E_2(R_1) = E_3(R_1) + E_4(R_1)$. The energy spectrum of electrons ejected at the second step of (10) was calculated using advanced adiabatic approximation, Eq. (3).

Our calculations have shown that the coupling of the states $2p\sigma^2$ and $1s\sigma 3d\sigma$ is strong and the parameter a equals 0.12 a.u. In order to obtain the true values of differential cross sections it is necessary to multiply Eqs. (3) and (4) by $P(v)$, Eq. (13). It should be noted that an important role of the correlated two-electron transitions in a population of excited states in HeE^+-He collisions was established earlier [31]. It must be emphasized that all of the parameters are calculated *ab initio* and no fitting parameters were used.

C. Quasimolecular autoionization

The following two channels for quasimolecular autoionization were considered:

$$(A1)\ 2p\sigma^2 \rightarrow 1s\sigma\varepsilon l\sigma, \quad l = 0,2, \quad (14)$$

$$(A2)\ 2p\sigma^2 \rightarrow 2p\sigma 2p\pi \rightarrow 1s\sigma\varepsilon d\pi. \quad (15)$$

Other autoionization transitions are much less important (as follows from the calculations [17]).

Channel (14) proceeds via decay of the initial diabatic state $2p\sigma^2$ that has survived after partial depletion via channel (10). Channel (15) proceeds in two steps: rotational excitation of the state $2p\sigma 2p\pi$ at small internuclear distances and subsequent autoionization of this state in departure of colliding particles.

Cross sections for electron ejection were calculated using expressions (3)–(8) with the functions $N(b,R)$ taken from the calculations [17] performed at close collision energy, accounting for proper statistical factors (statistical weights, numbers of electrons, and vacancies).

The results of calculations together with the experimental data on the doubly differential cross sections for electron ejection in 8 keV $^3He^{2+}$–^{4}He collisions are shown in Fig. 5. Agreement between the experimental data and calculations is good, indicating that the theory correctly describes the behavior and values of cross sections for different channels. As seen from the figure, the main contribution to the spectra at high electron energies is determined by autoionization channel A1, while channel D1 becomes dominant with decreasing electron energy. Other channels are not essential at the given ion energy. In general, the differential cross sections for electron ejection are mainly determined by the following three probabilities: (i) the probability for the discrete two-electron transition $2p\sigma^2$-$1s\sigma 3d\sigma$, (ii) the probability for the one-electron S promotion, and (iii) the probability for the quasimolecular autoionization $2p\sigma^2$-$1s\sigma\varepsilon l\sigma$. The first and third probabilities decrease with increasing ion energy while the second one grows with ion energy. Therefore, the ionization cross sections associated with the superposition of the three channels D1, A1, and A2 do not depend strongly on ion energy in the energy range under study. On the other hand, the cross sections for channels D2 and D3, Eq. (3), grow very strongly with ion energy and become comparable with other channels at ion energies of about several hundred keV.

D. Autoionization in separated atoms

Figure 6 shows a part of the energy spectrum associated with autoionization transitions in a separated target and projectile. As can be seen from the figure, most intensive spectral lines are attributed to decay of the states $2s^2\,^1S$, (33.2 eV), $2p^2\,^1D + 2s2p\,^1P$ (35.4 eV), and $2p^2\,^1S$ (37.5 eV), and less intensive lines, to decay of the states $2s3s\,^1S$ (38.3 eV) and $2s4s\,^1S$ (39.5 eV) (according to spectroscopic data [32]). Excitation of these states is connected with the population of molecular states $2s\sigma^2$, $2p\pi^2$, $2s\sigma 3d\sigma$, and $2s\sigma ns\sigma$ at small internuclear distances.

It is of interest to pay attention to very small cross sections for excitation of the atomic autoionization states. Such cross sections can be estimated by planimetry of the corresponding peaks in the energy spectrum. For example, the cross section for excitation of the state $2s^2$ is about 6×10^{-20} cm^2 at 10 keV, while the cross section for excitation of the molecular state $2s\sigma^2$ is about 4×10^{-18} cm^2, and the cross section for excitation of the state $2s^2$ in the system He^+-He is about 4×10^{-19} cm^2 [33]. (Note in the case of decay of the $2s^2$ state the corresponding peak is well resolved and the angular distribution of ejected s electrons is isotropic.) Our estimates show that the widths $\Gamma(R)$ for the $2s\sigma^2$ state are of the order of 10^{-3} a.u., which is far from being enough to explain such

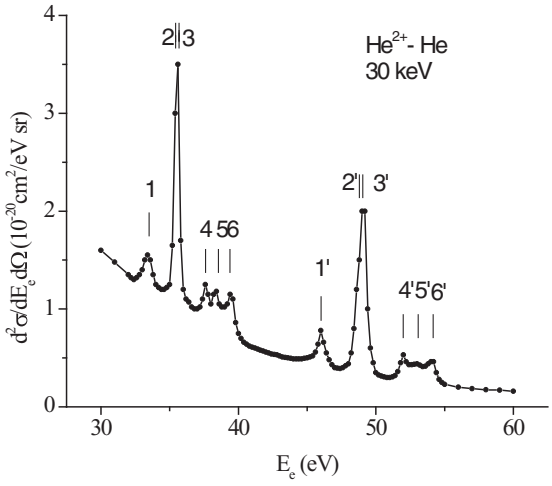

FIG. 6. Energy spectra of electrons ejected in decay of autoionization states of sepatated atoms. Autoionization states: 1, $2s^2\,^1S$; 2, $2p^2\,^1D$; 3, $2s2p\,^1P$; 4, $2p^2\,^1S$; 5, $2s3s\,^1S$; 6, $2s4s\,^1S$. The numbers with primes correspond to the same transitions in the projectile atom.

strong depletion of the above molecular state. Taking into account depletion via channel (10), 70% also does not help explain the observed effect. Such an explanation can be found in the assumption that the state $2s\sigma^2$ dissociates to $He^+(2s) + He^+(2s)$ at $R\to\infty$ (see, e.g., Ref. [15]) and the state $He^{2+} + He(2s^2)$ is produced via mixing with the above state. This idea is consistent with the "swapping" concept of Barat and Lichten [34]. Contrary to this situation, in the case of He^+-He the state $1s\sigma 2s\sigma^2$ converges to $He^+(1s)$-$He(2s^2)$, giving rise to enhancement of the cross section for excitation of the $2s^2$ state. A similar situation occurs in the case of other doubly excited autoionization states.

Meanwhile, the situation occurring in the COLTRIMS experiments is quite different. These experiments were performed at fixed values of the recoil momentum corresponding to the range of internuclear distances where channels (10)–(12) and (14) and (15) are closed and the rotational coupling between the states $2p\sigma^2$ (bound) and $2p\sigma 2p\pi$ (continuum) becomes dominant [17]. Then the excitation of the state $2p\sigma 2p\pi$ can be followed both by T ionization (saddle-point ionization) and by autoionization transition to the $1s\sigma$ state with ejection of π electrons. Such a picture is consistent with the findings of the COLTRIMS experiments.

VI. CONCLUSIONS

The data obtained in this work give a new insight into the problem of ionization in the system He_2^{2+} ($He^{2+} + He$). For the existence of an effective ionization channel, two-electron coupling followed by one-electron superpromotion at medium internuclear distances leads to considerable enhancement of cross sections in the keV ion energy range. This mechanism should be taken into account in the analysis of energy balance in helium plasmas.

In our previous work [35], it was shown that dynamical electron correlations give considerable contribution to electron detachment in negative ion–atom collisions. In the present study, another system, the multicharged ion–atom system, is found to undergo a strong influence of electron correlations. In particular, it has been shown that almost all significant ionization channels in keV-energy He^{2+}-He collisions are connected with electron correlation processes, both autoionization and discrete two-electron transitions. Thus, development of accurate theoretical programs for calculation of dynamical two-electron transitions in atomic collisions becomes very important. In the present case we have seen that a completely *ab initio* theory based on the advanced adiabatic approximation of Ref. [27] agrees well with our absolute measurements.

[1] S. Yu. Ovchinnikov, G. N. Ogurtsov, J. H. Macek, and Yu. S. Gordeev, Phys. Rep. **389**, 119 (2004).
[2] L. J. Puckett, G. O. Taylor, and D. W. Martin, Phys. Rev. **176**, 271 (1969).
[3] M. B. Shah and H. B. Gilbody, J. Phys. B **18**, 899 (1985).
[4] M. B. Shah, P. McCallion, and H. B. Gilbody, J. Phys. B **22**, 3037 (1989).
[5] V. V. Afrosimov, G. A. Leiko, Yu. A. Mamaev, and M. N. Panov, Sov. Phys. JETP **40**, 661 (1975).
[6] R. K. Janev, W. D. Langer, K. Evans, and D. E. Post, *Elementary Processes in Hydrogen-Helium Plasmas* (Springer-Verlag, Berlin, 1987).
[7] F. Frémont, A. Hajaji, A. Naja, C. Leclercq, J. Soret, J. A. Tanis, B. Suli, and J.-Y. Chesnel, Phys. Rev. A **72**, 050704(R) (2005).
[8] T. J. M. Zouros, D. Schneider, and N. Stolterfoht, Phys. Rev. A **35**, 1963 (1987).
[9] R. Dörner, V. Mergel, L. Zhaoyuan, J. Ullrich, L. Spielberger, R. E. Olson, and H. Schmidt-Böcking, J. Phys. B **28**, 435 (1995).
[10] V. Mergel *et al.*, Nucl. Instr. Methods Phys. Res. B **98**, 593 (1995).
[11] R. Dörner *et al.*, Nucl. Instr. Methods Phys. Res. B **99**, 111 (1995).
[12] M. Abdallah, S. Kravis, C. L. Cocke, Y. Wang, V. D. Rodriguez, and M. Stöckli, Phys. Rev. A **56**, 2000 (1997).
[13] M. Abdallah, C. L. Cocke, W. Wolff, H. Wolff, S. D. Kravis, M. Stöckli, and E. Kamber, Phys. Rev. Lett. **81**, 3627 (1998).
[14] M. Schulz and D. H. Madison, Int. J. Mod. Phys. A **21**, 3649 (2006).
[15] H. Yagisawa, H. Sato, and T. Watanabe, Phys. Rev. A **16**, 1352 (1977).
[16] V. K. Nikulin and N. A. Guschina, J. Phys. B **11**, 3553 (1978).
[17] S. Hara and H. Sato, J. Phys. B **11**, 955 (1978).
[18] F. Koike, H. Nakamura, S. Hara, Y. Itikawa, M. Matsuzawa, H. Sato, and I. Shimamura, J. Phys. B **11**, 4193 (1978).
[19] H. Sato and S. Hara, J. Phys. B **13**, 4577 (1980).
[20] M. Aubert-Frecon, P. Ceyzeriat, A.-M. Jorus, and C. Lesech, J. Phys. B **17**, L7 (1984).
[21] S. Hara and H. Sato, J. Phys. B **17**, 4301 (1984).
[22] G. N. Ogurtsov, A. G. Kroupyshev, M. G. Sargsyan, Yu. S. Gordeev, and S. Yu. Ovchinnikov, Phys. Rev. A **53**, 2391 (1996).
[23] G. N. Ogurtsov, J. Phys. B **31**, 1805 (1998).
[24] C. B. Opal, E. C. Beaty, and W. K. Peterson, At. Data Nucl. Data Tables **4**, 209 (1972).
[25] S. Yu. Ovchinnikov and J. H. Macek, Phys. Rev. A **55**, 3605 (1997).
[26] F. Koike, M. Matsuzawa, S. Hara, Y. Itikawa, H. Nakamura, H. Sato, and I. Shimamura, J. Phys. B **12**, 2325 (1979).
[27] S. Yu. Ovchinnikov and E. A. Solov'ev, Zh. Eksp. Teor. Fiz. **91**, 477 (1986).
[28] G. Gerber and A. Niehaus, J. Phys. B **9**, 123 (1976).
[29] G. N. Ogurtsov, S. Yu. Ovchinnikov, and V. M. Mikoushkin, Phys. Scr., T **110**, 370 (2004)
[30] E. A. Solov'ev, Sov. Phys. Usp. **32**, 288 (1989).
[31] J. C. Brenot, D. Dhuicq, J. P. Gauyacq, J. Pommier, V. Sidis, M. Barat, and E. Pollack, Phys. Rev. A **11**, 1245 (1975).
[32] P. J. Hicks and J. Comer, J. Phys. B **8**, 1866 (1975).
[33] A. Bordenave-Montesquieu, A. Gleizes, and P. Benoit-Cattin, Phys. Rev. A **25**, 245 (1982).
[34] M. Barat and W. Lichten, Phys. Rev. A **8**, 211 (1972).
[35] G. N. Ogurtsov, V. M. Mikoushkin, S. Yu. Ovchinnikov, and J. H. Macek, Phys. Rev. A **74**, 042720 (2006).